Supporting Information

Confining Hyperbranched Star Poly(ethylene oxide)-Based Polymer into 3D Interpenetrating Network for High Performance All-Solid-State Polymer Electrolyte

Pingping Chen,[a] Xu Liu,[a] Shi Wang,[a] Qinghui Zeng,[a] Zhinan Wang,[a] Zengxi Li,*[,a] and Liaoyun Zhang*[,a]

[a] School of Chemical Sciences, University of Chinese Academy of Sciences, Beijing 100049, China.

* Correspondence*:* zhangly@ucas.ac.cn; Lizengxi@ucas.ac.cn.

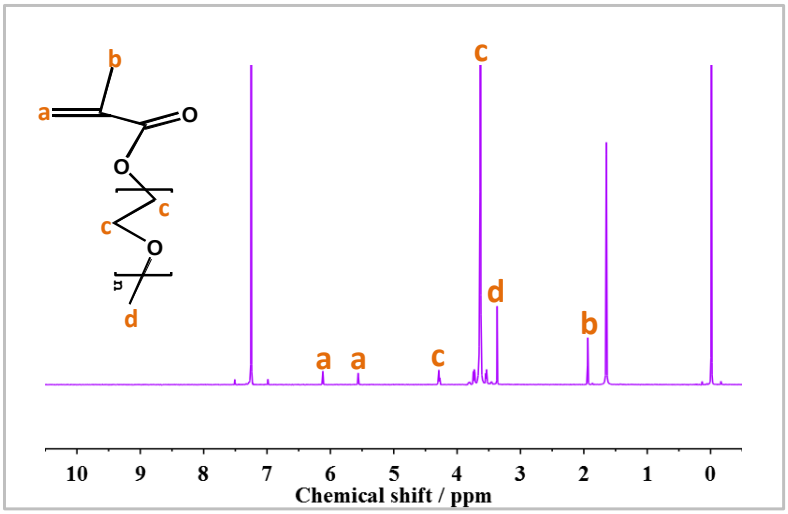

Figure S1. H^1 NMR spectrum of PEGMA.

Table S1. The GPC results of the prepared HBPS and HSP.

Polymer	M_n	M_w	M_p	M_z	PDI
HBPS	41504	92692	57091	207502	2.23
HSP	456137	571688	367994	731042	1.25

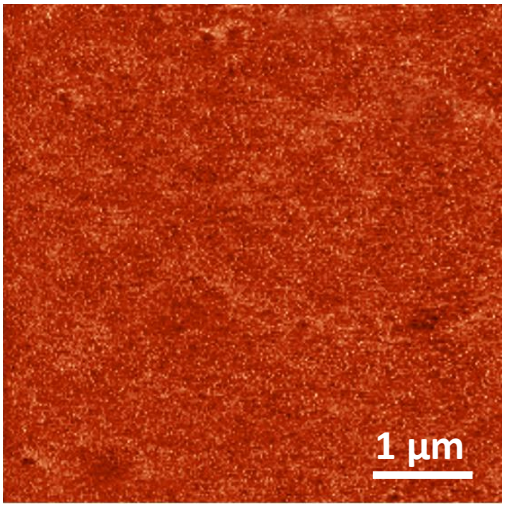

Figure S2. Tapping mode AFM phase image of HPEA-40 membrane.

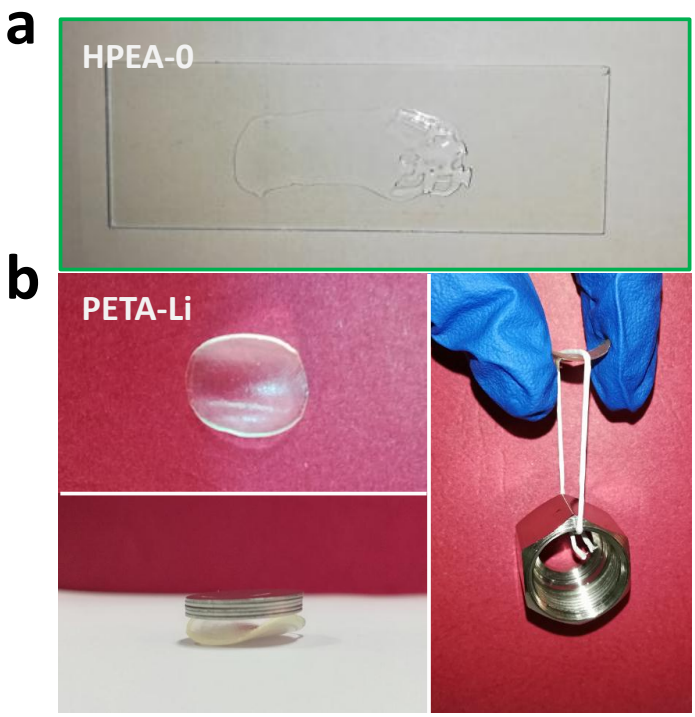

Figure S3. Photographs of (a) HPEA-0 and (b) PETA-Li membrane.

The HPEA-0 membrane represents the membrane prepared without the cross-linker, and as shown in Fig. S3a, the HPEA-0 polymer electrolyte showed inferior film-forming capability due to its highly branched structure and the strong plasticizing effect of LiTFSI. Additionally, the pure PETA membrane was brittle because of its rigid 3D network structure, and after adding certain amount of LiTFSI, the PETA-Li membrane demonstrated enough toughness and strength to endure the external pressure as showed from Fig. S3b.

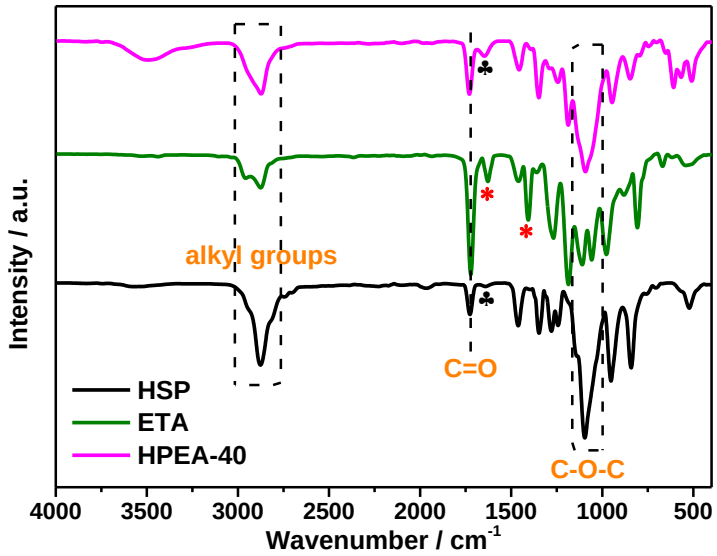

Figure S4. FT-IR spectra of HSP, ETA and HPEA-40 membrane.

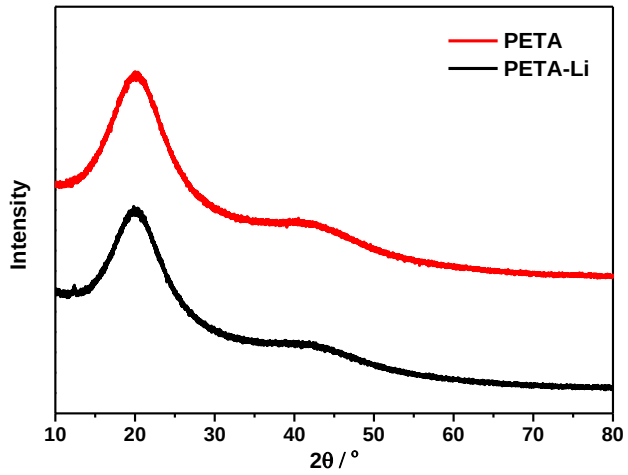

Figure S5. XRD patterns of PETA and PETA-Li membrane.

Due to the tough and compact 3D network structure created by the cross-linker, the polymerized ETA membranes showed similar crystalline peaks for PETA and PETA-Li.

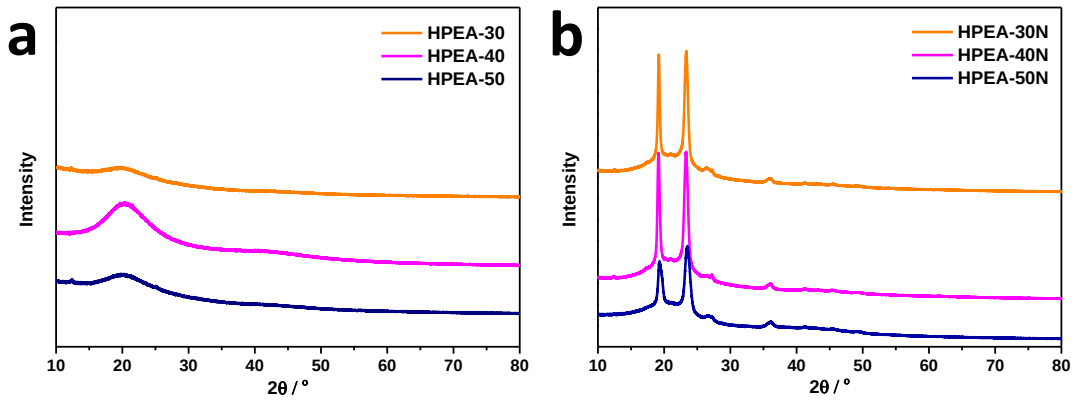

Figure S6. XRD patterns of HPEA based membranes with different cross-linker content (a) with LiTFSI and (b) without LiTFSI.

The HPEA-XN (X = 30, 40, and 50) in the Fig. S6b represent the corresponding polymer electrolyte prepared without the addition of LiTFSI. From Fig. S6a and b, it can be seen that increasing the cross-linker content will lead to effectively decreased crystalline degree of HPEA membrane. The conclusion could be further confirmed by the results of SAXS in Fig. S7.

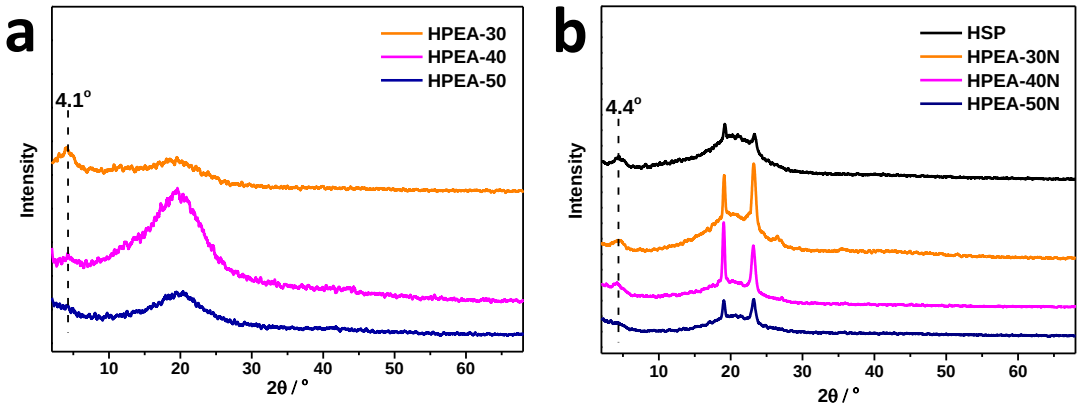

Figure S7. SAXS patterns of HPEA based membranes with different cross-linker content (a) with LiTFSI and (b) without LiTFSI.

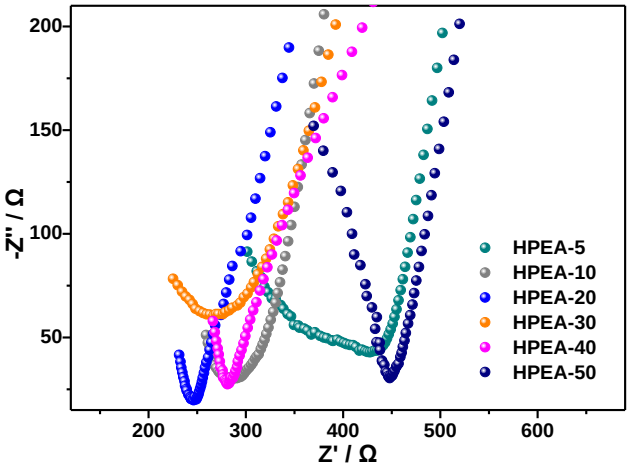

Figure S8. EIS spectra of HPEA based membranes with different cross-linker content at 50 ^{o}C.

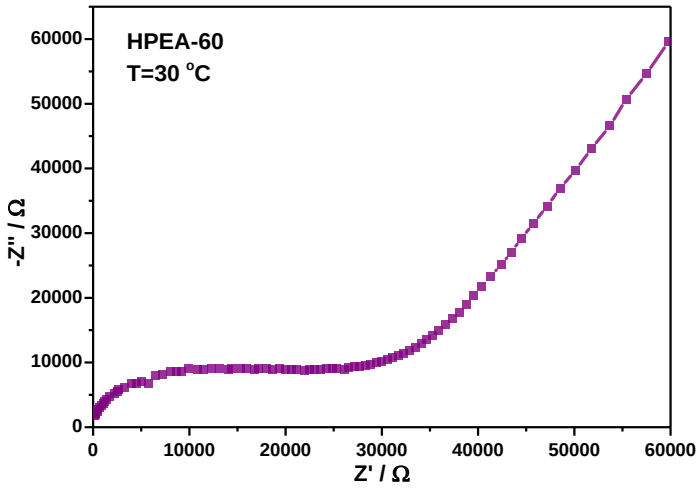

Figure S9. Impedance spectroscopy of HPEA-60 membrane at 30 °C.

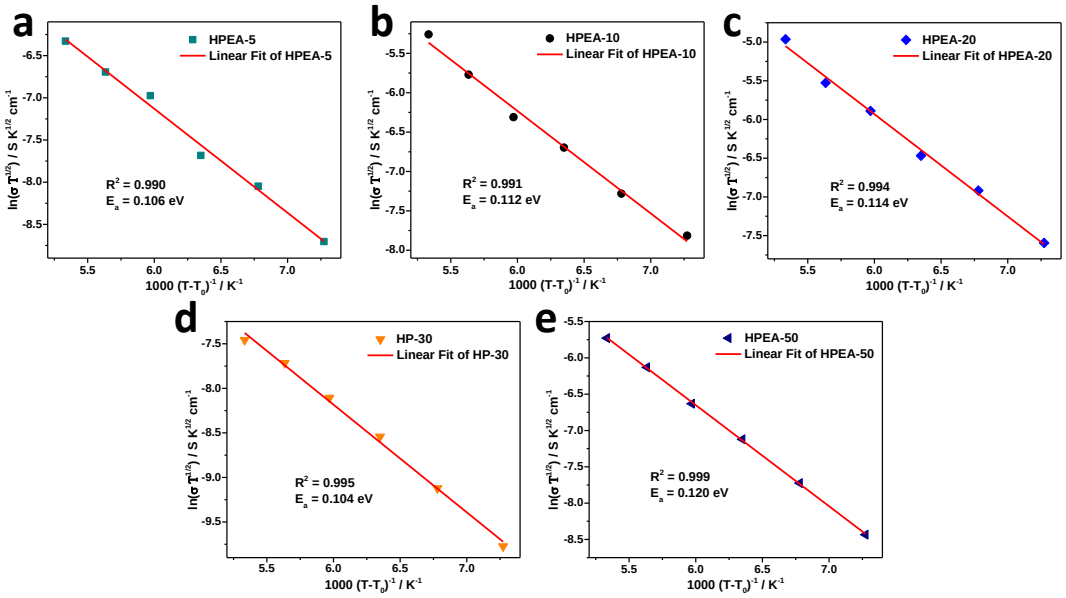

Figure S10. VTF plots of (a) HPEA-5, (b) HPEA-10, (c) HPEA-20, (d) HPEA-30, and (e) HPEA-50 membranes.

The VTF equation can be expressed by Eq. (1)[1]

$$\sigma = \sigma_0 T^{-\frac{1}{2}} \exp\left(-\frac{E_a}{T - T_0}\right) \qquad (1)$$

where σ_0 is the pre-exponential factor, E_a is the activation energy, and T_0 is the ideal glass transition temperature which is normally 10-50 K below the experimental glass transition temperature. In the total calculation process, the values of T_g for all the polymer electrolytes were approximately -57.5 ^{o}C, and $T_0 = T_g - 50$ K.

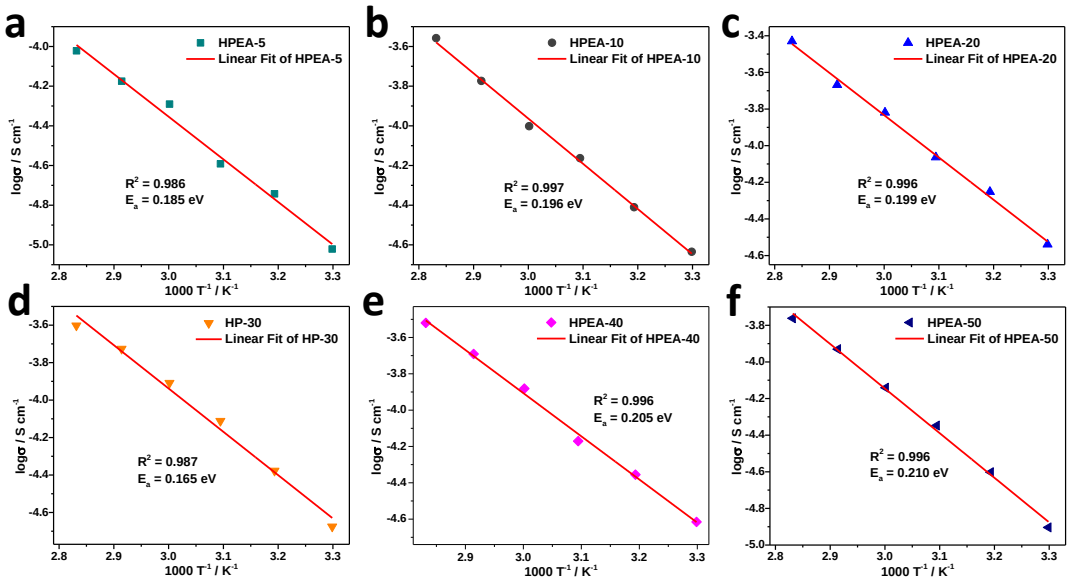

Figure S11. Arrehenius plots of (a) HPEA-5, (b) HPEA-10, (c) HPEA-20, (d) HPEA-30, (e) HPEA-40, and (f) HPEA-50 membranes.

The Arrhenius equation can be expressed by Eq. (2)[2]

$$\sigma = \sigma_0 \exp\left(\frac{-E_a}{kT}\right) \qquad (2)$$

where σ_0 is the pre-exponential factor, E_a is the activation energy, and k is the Boltzmann constant.

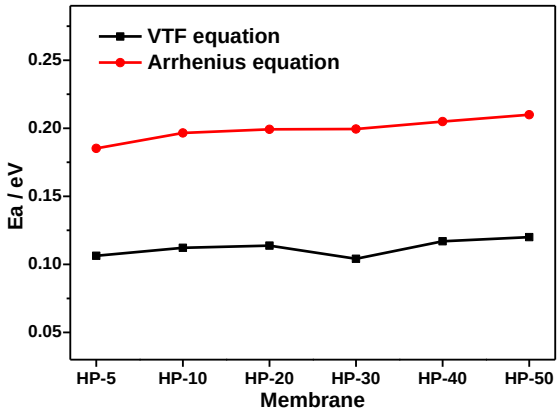

Figure S12. The activation energy, E_a, of HPEA based polymer electrolytes calculated by the VTF equation and the Arrhenius equation, respectively.

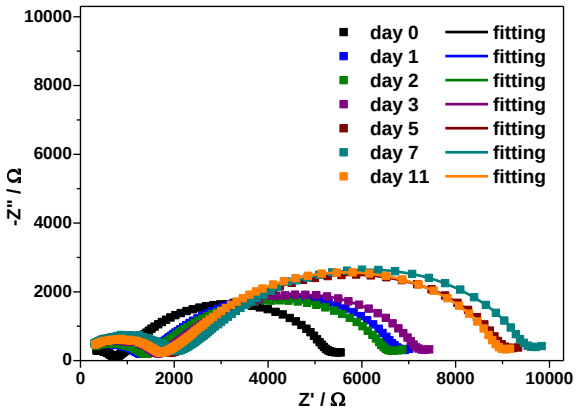

Figure S13. Impedance spectra for Li/HPEA-40/Li cell at room temperature.

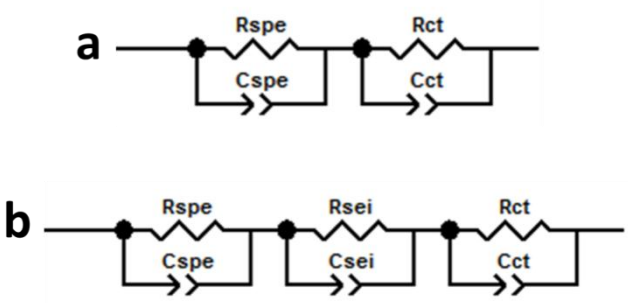

Figure S14. Equivalent circuit models for Li/HPEA-40/Li symmetric cell: (a) the initial stage and (b) successive stage.

Table S2. The Fitting results of EIS analyses for Li/HPEA-40/Li symmetric cell during storage process.

R	0 d	1 d	2 d	3 d	5 d	7 d	11 d
R_{SPE} / Ω	767	1165	1277	1565	1836	1875	1592
C_{SPE} / F	6.7E-09	2.6E-09	4.3E-09	3.9E-09	3.7E-09	4.3E-09	4.2E-09
R_{SEI} / Ω	—	2470	2282	2420	3097	3090	2495
C_{SEI} / F	—	2.6E-05	3.0E-05	2.5E-05	2.1E-05	2.6E-05	2.8E-05
R_{CT} / Ω	4644	3521	3329	3537	4471	4974	5147
C_{CT} / F	2.4E-06	1.9E-06	2.6E-06	2.8E-06	2.8E-06	2.7E-06	2.8E-06

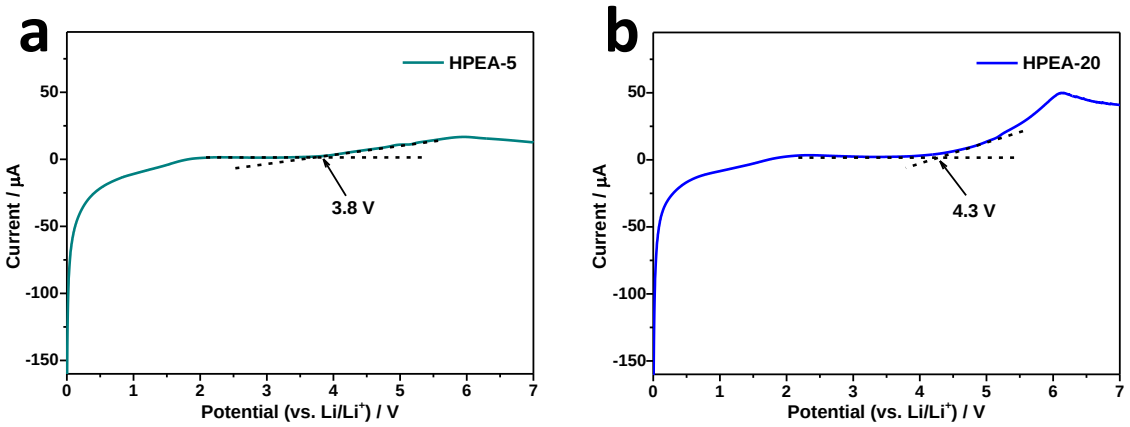

Figure S15. Linear sweep voltammetry curves of (a) HPEA-5 and (b) HPEA-20 membranes at a scanning rate of 3 mV s^{-1} at room temperature.

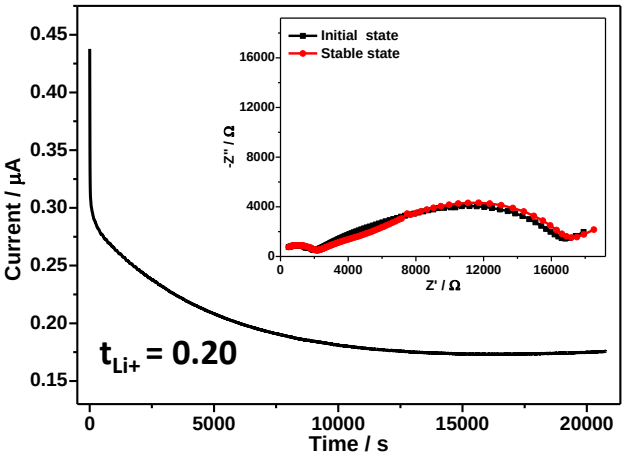

Figure S16. Chronoamperometry profiles and the inset shows AC impedance spectra before and after polarization for symmetric Li/HPEA-40/Li cell at room temperature.

The lithium ion transfer number was calculated by Bruce-Vincent-Evans equation:[3]

$$t_{Li^+} = \frac{I_{ss}(\Delta V - I_0 R_0)}{I_0(\Delta V - I_{ss} R_{ss})}$$

ΔV is polarization voltage (10 mV), I_0 and R_0 are the initial current and interfacial resistance before polarization, and I_{ss} and R_{ss} are the steady current and interfacial resistance, respectively.

Table S3. Comparisons of ionic conductivity and electrochemical stability window for the different PEO-based polymer electrolytes.

PEO based SPE	Temperature / °C	Ionic conductivity / S cm^{-1}	Electrochemical window / V	Reference
PEO-TEGDMA-TEGDME	24	2.7×10^{-4}	5.0	4
PEO@CMOF	25	3.2×10^{-5}	4.9	5
K-SPE750-Li	20	2.8×10^{-5}	5.3	6
PEO-PEA@liquid electrolyte	25	2.2×10^{-3}	4.5	7
PEO@C_3N_4	30	2.3×10^{-6}	4.7	3
PEO-PEGDA-DVB	25	1.0×10^{-6}	4.3	8
PEO@MOF-5	25	3.2×10^{-5}	4.6	9
PEO-KH560	25	3.2×10^{-5}	4.9	10
HPEA-40	30	2.4×10^{-5}	5.1	this work

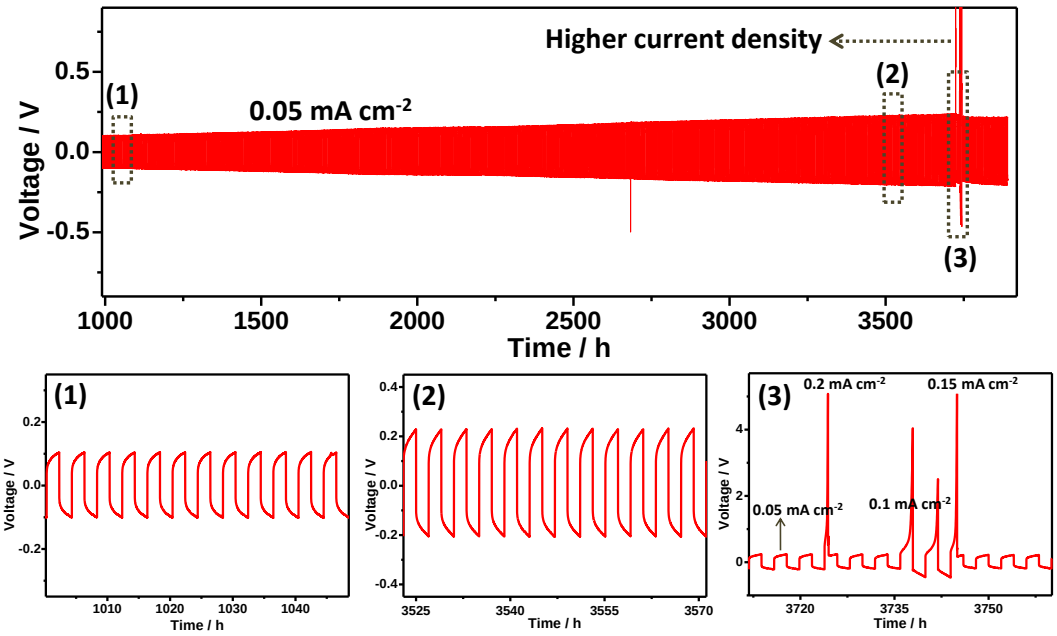

Figure S17. Galvanostatic cycling of Li/HPEA-40/Li cell at 50 ^{o}C and different current density.

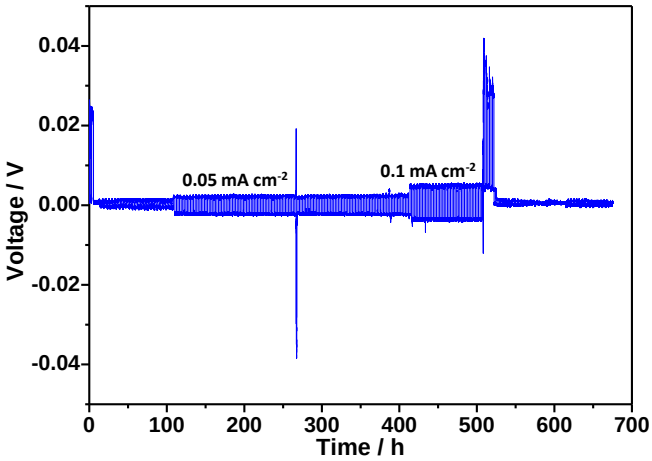

Figure S18. Galvanostatic cycling of Li/liquid electrolyte/Li cell at 50 ^{o}C and different current density.

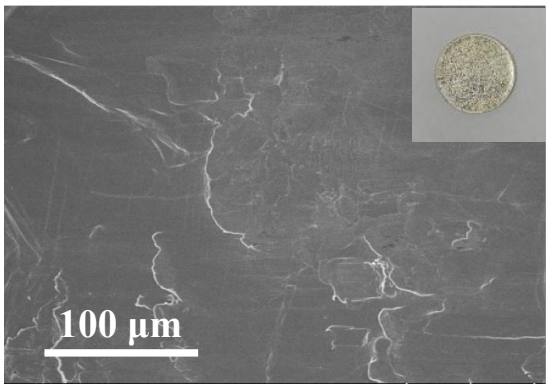

Figure S19. The surface SEM image of fresh Li metal, and the inset is the photograph of Li metal with bright lustre.

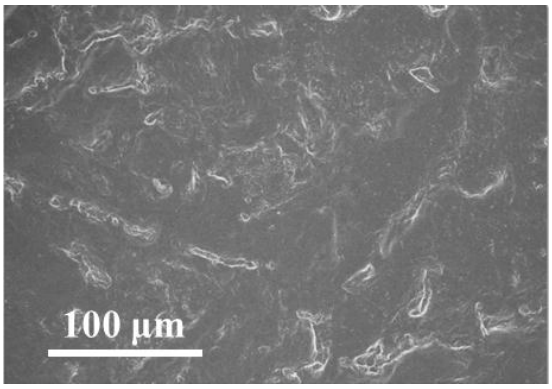

Figure S20. Plane-view SEM image of HPEA-40 membrane after over 200 cycles for symmetric Li/HPEA-40/Li cell.

Compared with the fresh polymer electrolyte shown in Fig. 1d, the cycled HPEA-40 membrane in symmetric Li/HPEA-40/Li cell nearly maintained the original morphology, and a small number of particles on the surface of membrane were residual lithium dendrites after disassembling the cell.

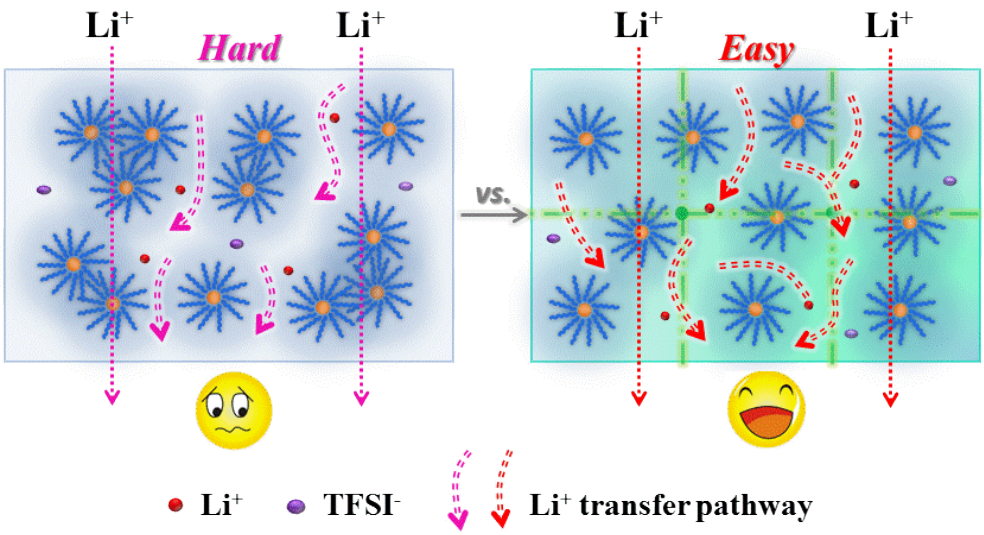

Figure S21. The comparative schematic of ion transport mechanism in HPEA based polymer electrolytes without (the left) or with (the right) the cross-linker.

The cross-linker played the two main functions on the performance enhancement of the polymer electrolyte. On one hand, the cross-linker provided the HSP with 3D interpenetrating hard network, enabling the polymer electrolyte to obtain good film-forming capability and dendrite-inhibiting ability. On the other hand, the cross-linker decreased the crystalline degree of polymer electrolyte and sped up polymer chain segmental dynamics, thus effectively improving ionic conductivity of electrolyte.

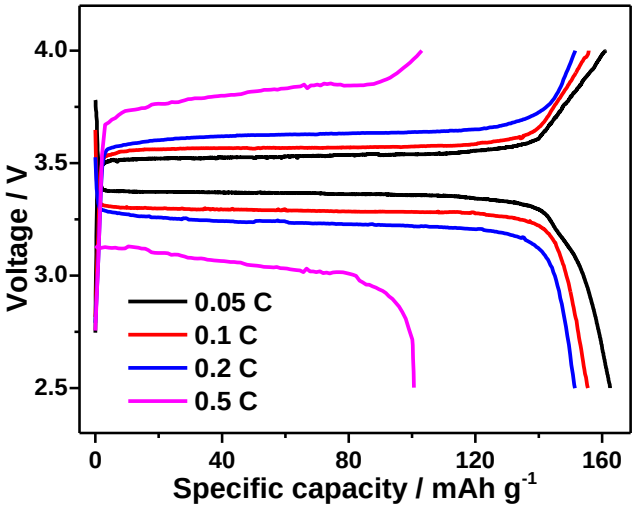

Figure S22. Charge-discharge profiles at different rates at 50 ^{o}C with HPEA-40 polymer electrolyte.

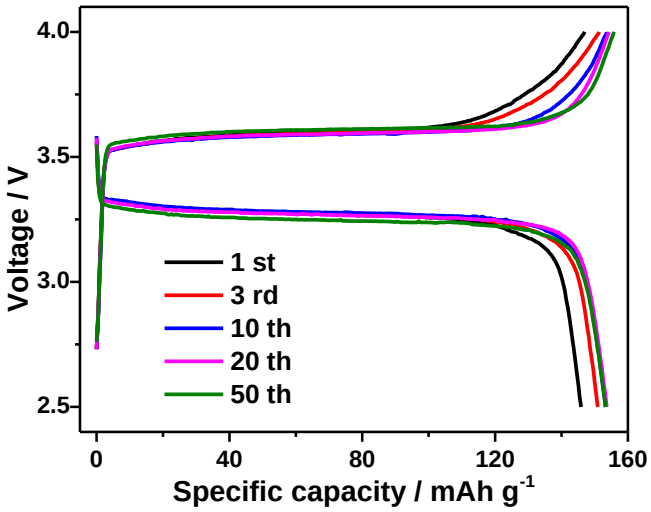

Figure S23. Charge-discharge profiles at 0.2 C at 50 ^{o}C for LFP/HPEA-40/Li cell.

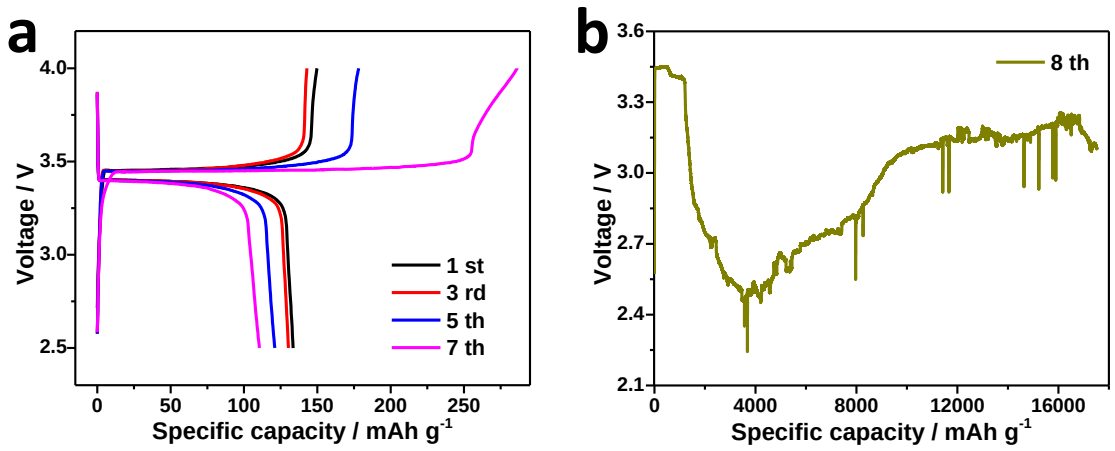

Figure S24. Charge-discharge profiles at 0.2 C at 50 ^{o}C (a) at 7 cycles and (b) at 8th cycle for LFP/liquid electrolyte/Li cell.

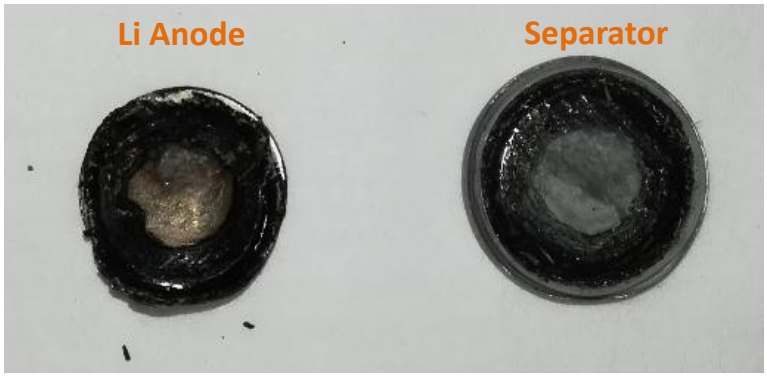

Figure S25. Photographs of Li anode and separator from the cycled LFP/liquid electrolyte/Li cell at 50 ^{o}C.

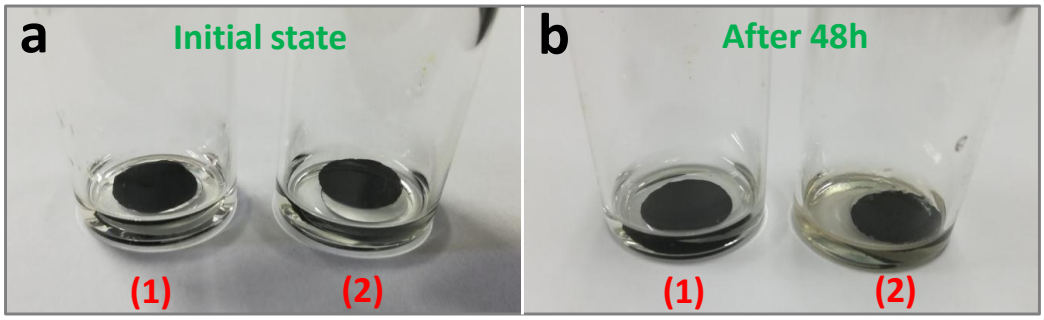

Figure S26. The photographs of the LFP cathodes when immersed into liquid electrolytes at the initial stage (a) and after 48 h (b); the sample (1) is kept at room temperature and the sample (2) is kept at 50 ^{o}C.

Figures S25 and S26 showed that there were undesirable sides reactions inside the LFP/liquid electrolyte/Li cell when operated at 50 ^{o}C, including the decomposition of the cathode materials and passivation film on the anode and the reaction between lithium metal and organic solvents, which were responsible for the failure of liquid cell.

Supplementary References:

[1] Luo, J.; Conrad, O.; Vankelecom, I. Physicochemical Properties of Phosphonium-Based and Ammonium-Based Protic Ionic Liquids. *J. Mater. Chem.* **2012**, *22*, 20574-20579.

[2] Song, S.; Wu, Y.; Tang, W.; Deng, F.; Yao, J.; Liu, Z.; Hu, R.; Alamusi; Wen, Z.; Lu, L.; Hu, N. Composite Solid Polymer Electrolyte with Garnet Nanosheets in Poly(ethylene oxide). *ACS Sustainable Chem. Eng.* **2019**, *7*, 7163-7170.

[3] Sun, Z.; Li, Y.; Zhang, S.; Shi, L.; Wu, H.; Bu, H.; Ding, S. g-C_3N_4 Nanosheets Enhanced Solid Polymer Electrolytes with Excellent Electrochemical Performance, Mechanical Properties, and Thermal Stability. *J. Mater. Chem. A* **2019**, *7*, 11069-11076.

[4] Zhang, Y.; Lu, W.; Cong, L.; Liu, J.; Sun, L.; Mauger, A.; Julien, C.; Xie, H.; Liu, J. Cross-Linking Network Based on Poly(ethylene oxide): Solid Polymer Electrolyte for Room Temperature Lithium Battery. *J. Power Sources* **2019**, *420*, 63-72.

[5] Huo, H.; Wu, B.; Zhang, T.; Zheng, X.; Ge, L.; Xu, T.; Guo, X.; Sun, X. Anion-Immobilized Polymer Electrolyte Achieved by Cationic Metal-Organic Framework Filler for Dendrite-Free Solid-State Batteries. *Energy Storage Materials* **2019**, *18*, 59-67.

[6] Xiao, Z.; Zhou, B.; Wang, J.; Zuo, C.; He, D.; Xie, X.; Xue, Z. PEO-Based Electrolytes Blended with Star Polymers with Precisely Imprinted Polymeric Pseudo-Crown Ether Cavities for Alkali Metal Ion Batteries. *J. Membrane Sci.* **2019**, *576*, 182-189.

[7] Zeng, X.; Yin, Y.; Li, N.; Du, W.; Guo, Y.; Wan, L. Reshaping Lithium Plating/Stripping Behavior via Bifunctional Polymer Electrolyte for Room-Temperature Solid Li Metal Batteries. *J. Am. Chem. Soc.* **2016**, *138*, 15825-15828.

[8] Ben, H.; Garcia-Calvo, O.; Lago, N.; Devaraj, S.; Armand, M. Cross-Linked Solid Polymer Electrolyte for All-Solid-State Rechargeable Lithium Batteries. *Electrochim. Acta* **2016**, *220*, 587-594.

[9] Yuan, C.; Li, J.; Han, P.; Lai, Y.; Zhang, Z.; Liu, J. Enhanced Electrochemical Performance of Poly(ethylene oxide) Based Composite Polymer Electrolyte by Incorporation of Nano-Sized Metal-Organic Framework. *J. Power Sources* **2013**, *240*, 653-658.

[10] Han, P.; Zhu, Y.; Liu, J. An All-Solid-State Lithium Ion Battery Electrolyte Membrane Fabricated by Hot-Pressing Method. *J. Power Sources* **2015**, *284*, 459-465.